Influence of temperature on the molecular composition of ions and charged clusters during pure biogenic nucleation

Carla Frege[1], Ismael K. Ortega[2], Matti P. Rissanen[3], Arnaud P. Praplan[3], Gerhard Steiner[3,4,5], Martin Heinritzi[6], Lauri Ahonen[3], António Amorim[7], Anne-Kathrin Bernhammer[4], Federico Bianchi[1,3], Sophia Brilke[4], Martin Breitenlechner[4], Lubna Dada[3], António Dias[7], Jonathan Duplissy[3,8], Sebastian Ehrhart[8], Imad El-Haddad[1], Lukas Fischer[4], Claudia Fuchs[1], Olga Garmash[3], Marc Gonin[9], Armin Hansel[4], Christopher R. Hoyle[1], Tuija Jokinen[3], Heikki Junninen[3], Jasper Kirkby[6,8], Andreas Kürten[6], Katrianne Lehtipalo[1,3], Markus Leiminger[6], Roy Lee Mauldin[3,16], Ugo Molteni[1], Leonid Nichman[10], Tuukka Petäjä[3], Nina Sarnela[3], Siegfried Schobesberger[3], Mario Simon[6], Mikko Sipilä[3], Dominik Stolzenburg[5], António Tomé[11], Alexander L. Vogel[1,8], Andrea Wagner[6], Robert Wagner[3], Mao Xiao[1], Chao Yan[3], Penglin Ye[12,15], Joachim Curtius[4], Neil M. Donahue[12], Rick C. Flagan[13], Markku Kulmala[3], Douglas R. Worsnop[3,14,15], Paul M. Winkler[5], Josef Dommen[1] and Urs Baltensperger[1]

[1] Paul Scherrer Institute, Laboratory of Atmospheric Chemistry, CH-5232 Villigen, Switzerland
[2] Onera -The French Aerospace Lab, F-91123 Palaiseau, France
[3] University of Helsinki, Department of Physics, P.O.Box 64, 00014 University of Helsinki, Finland
[4] University of Innsbruck, Institute of Ion Physics and Applied Physics, Technikerstraße 25, 6020 Innsbruck, Austria
[5] University of Vienna, Faculty of Physics, Boltzmanngasse 5, 1090 Vienna, Austria
[6] Institute for Atmospheric and Environmental Sciences, Goethe University Frankfurt, 60438 Frankfurt am Main, Germany
[7] Universidade de Lisboa, Ed. C8, Campo Grande, Lisboa- 1749-016, Portugal
[8] CERN, CH-1211 Geneva, Switzerland
[9] Tofwerk AG, 3600 Thun, Switzerland
[10] School of Earth and Environmental Sciences, University of Manchester, Manchester M13 9PL, UK
[11] IDL -Universidade da Beira Interior, Av. Marquês D'Avila e Bolama, 6201-001 Covilhã, Portugal.
[12] Center for Atmospheric Particle Studies, Carnegie Mellon University, Pittsburgh, Pennsylvania 15213, USA

[13] Division of Chemistry and Chemical Engineering, California Institute of Technology, Pasadena, California 91125, USA

[14] University of Eastern Finland, FI-70211 Kuopio, Finland

[15] Aerodyne Research Inc., Billerica, Massachusetts 01821, USA

[16] Department of Atmospheric and Oceanic Sciences, University of Colorado, Boulder, Colorado 80309-0311, USA.

Abstract

It was recently shown by the CERN CLOUD experiment that biogenic highly oxygenated molecules (HOMs) form particles under atmospheric conditions in the absence of sulfuric acid where ions enhance the nucleation rate by one to two orders of magnitude. The biogenic HOMs were produced from ozonolysis of α-pinene at 5°C. Here we extend this study to compare the molecular composition of positive and negative HOM clusters measured with atmospheric pressure interface time-of-flight mass spectrometers (APi-TOFs), at three different temperatures (25°C, 5°C and -25°C). Most negative HOM clusters include a nitrate (NO_3^-) ion and the spectra are similar to those seen in the nighttime boreal forest. On the other hand, most positive HOM clusters include an ammonium (NH_4^+) ion and the spectra are characterized by mass bands that differ in their molecular weight by ~20 C atoms, corresponding to HOM dimers. At lower temperatures the average oxygen to carbon (O:C) ratio of the HOM clusters decreases for both polarities, reflecting an overall reduction of HOM formation with decreasing temperature. This indicates a decrease in the rate of autoxidation with temperature due to a rather high activation energy as has previously been determined by quantum chemical calculations. Furthermore, at the lowest temperature (-25°C) the presence of C_{30} clusters show that HOM monomers start to contribute to the nucleation of positive clusters. These experimental findings are supported by quantum chemical calculations of the binding energies of representative neutral and charged clusters.

1. Introduction

Atmospheric aerosol particles directly affect climate by influencing the transfer of radiant energy through the atmosphere (Boucher et al., 2013). In addition, aerosol particles can

68   indirectly affect climate, by serving as cloud condensation nuclei (CCN) and ice nuclei (IN).

69   They are of natural or anthropogenic origin, and result from direct emissions (primary

70   particles) or from oxidation of gaseous precursors (secondary particles). Understanding

71   particle formation processes in the atmosphere is important since more than half of the

72   atmospheric aerosol particles may originate from nucleation (Dunne et al., 2016; Merikanto

73   et al., 2009).

74   Due to its widespread presence and low saturation vapor pressure, sulfuric acid is believed to

75   be the main vapor responsible for new particle formation (NPF) in the atmosphere. Indeed,

76   particle nucleation is dependent on its concentration, albeit with large variability (Kulmala et

77   al., 2004). The combination of sulfuric acid with ammonia and amines increases nucleation

78   rates due to a higher stability of the initial clusters (Almeida et al., 2013; Kirkby et al., 2011;

79   Kürten et al., 2016). However, these clusters alone cannot explain the particle formation rates

80   observed in the atmosphere. Nucleation rates are greatly enhanced when oxidized organics

81   are present together with sulfuric acid, resulting in NPF rates that closely match those

82   observed in the atmosphere (Metzger et al., 2010; Riccobono et al., 2014). An important

83   characteristic of the organic molecules participating in nucleation is their high oxygen content

84   and consequently low vapor pressure. The formation of these highly oxygenated molecules

85   (HOMs) has been described by Ehn et al. (2014), who found that, following the well-known

86   initial steps of α-pinene ozonolysis through a Criegee intermediate leading to the formation of

87   an $RO_2\cdot$ radical, several repeated cycles of intramolecular hydrogen abstractions and O_2

88   additions produce progressively more oxygenated $RO_2\cdot$ radicals, a mechanism called

89   autoxidation (Crounse et al., 2013). The (extremely) low volatility of the HOMs results in

90   efficient NPF and growth, even in the absence of sulfuric acid (Kirkby et al., 2016; Tröstl et

91   al., 2016). The chemical composition of HOMs during NPF has been identified from α-

92   pinene and pinanediol oxidation by Praplan et al. (2015) and Schobesberger et al. (2013),

93   respectively.

94   Charge has also been shown to enhance nucleation (Kirkby et al., 2011). Ions are produced

95   in the atmosphere mainly by galactic cosmic rays and radon. The primary ions are N^+, N_2^+,

96   O^+, O_2^+, H_3O^+, O^- and O_2^- (Shuman et al., 2015). These generally form clusters with water

97   (e.g. $(H_2O)H_3O^+$) and after further collisions the positive and negative charges are transferred

98   to trace species with highest and lowest proton affinities, respectively (Ehn et al., 2010). Ions

99   are expected to promote NPF by increasing the cluster binding energy and reducing

100   evaporation rates (Hirsikko et al., 2011). Recent laboratory experiments showed that ions

101   increase the nucleation rates of HOMs from the oxidation of α-pinene by one to two orders of

102   magnitude compared to neutral conditions (Kirkby et al. 2016). This is due to two effects, of

103   which the first is more important: 1) an increase in cluster binding energy, which decreases

104   evaporation and 2) an enhanced collision probability, which increases the condensation of

105   polar vapors on the charged clusters (Lehtipalo et al., 2016; Nadykto, 2003).

106   Temperature plays an important role in nucleation, resulting in strong variations of NPF

107   at different altitudes. Kürten et al. (2016) studied the effect of temperature on nucleation for

108   the sulfuric acid - ammonia system, finding that low temperatures decrease the needed

109   concentration of H_2SO_4 to maintain a certain nucleation rate. Similar results have been found

110   for sulfuric acid − water binary nucleation (Duplissy et al., 2016; Merikanto et al., 2016),

111   where temperatures below 0˚C were needed for NPF to occur at atmospheric concentrations.

112   Up to now, no studies have addressed the temperature effect on NPF driven by HOMs from

113   biogenic precursors such as α-pinene.

114   In this study we focus on the chemical characterization of the ions and the influence of

115   temperature on their chemical composition during organic nucleation in the absence of

116   sulfuric acid. The importance of such sulfuric acid-free clusters for NPF has been shown in

117   the laboratory (Kirkby et al., 2016; Tröstl et al., 2016) as well as in the field (Bianchi et al.,

118   2016). We present measurements of the NPF process from the detection of primary ions (e.g.

119   N_2^+, O_2^+, NO^+) to the formation of clusters in the size range of small particles, all under

120   atmospherically relevant conditions. The experiments were conducted at three different

121   temperatures (-25, 5 and 25 ˚C) enabling the simulation of pure biogenic NPF representative

122   of different tropospheric conditions. This spans the temperature range where NPF might

123   occur in tropical or sub-tropical latitudes (25 °C), high-latitude boreal regions (5 °C) and the

124   free troposphere (-25 °C). For example, NPF events were reported to occur in an Australian

125   Eucalypt forest (Suni et al., 2008) and the boreal station in Hyytiala (Kulmala et al., 2013).

126   Nucleation by organic vapors was also observed at a high mountain station (Bianchi et al,

127   2016). High aerosol particle concentrations were measured in the upper troposphere over the

128   Amazon Basin and tentatively attributed to the oxidation of biogenic volatile organic

129   compounds (Andreae et al., 2017).

130

2. Methods

2.1. The CLOUD chamber

We conducted experiments at the CERN CLOUD chamber (Cosmics Leaving Outdoor Droplets). With a volume of 26.1 m^3, the chamber is built of electropolished stainless steel and equipped with a precisely controlled gas system. The temperature inside the chamber is measured with a string of six thermocouples (TC, type K) which were mounted horizontally between the chamber wall and the center of the chamber at distances of 100, 170, 270, 400, 650, and 950 mm from the chamber wall (Hoyle et al., 2016). The temperature is controlled accurately (with a precision of $\pm$ 0.1°C) at any tropospheric temperature between -65 and 30 °C (in addition, the temperature can be raised to 100 °C for cleaning). The chamber enables atmospheric simulations under highly stable experimental conditions with low particle wall loss and low contamination levels (more details of the CLOUD chamber can be found in Kirkby et al. (2011) and Duplissy et al. (2016)). At the beginning of the campaign the CLOUD chamber was cleaned by rinsing the walls with ultra-pure water, followed by heating to 100˚C and flushing at a high rate with humidified synthetic air and elevated ozone (several ppmv) (Kirkby et al., 2016). This resulted in SO_2 and H_2SO_4 concentrations that were below the detection limit (<15 pptv and $<5 \times 10^4$ cm^{-3}, respectively), and total organics (largely comprising high volatility C_1–C_3 compounds) that were below 150 pptv.

The air in the chamber is ionized by galactic cosmic rays (GCR); higher ion generation rates can be induced by a pion beam (π^+) from the CERN Proton Synchrotron enabling controlled simulation of galactic cosmic rays throughout the troposphere. Therefore, the total ion-pair production rate in the chamber is between 2 (no beam) and 100 cm^{-3} s^{-1} (maximum available beam intensity, Franchin et al., 2015).

2.2. Instrumentation

The main instruments employed for this study were atmospheric pressure interface time-of-flight (APi-TOF, Aerodyne Research Inc. & Tofwerk AG) mass spectrometers. The instrument has two main parts. The first is the atmospheric pressure interface (APi) where ions are transferred from atmospheric pressure to low pressures via three differentially

159   pumped vacuum stages. Ions are focused and guided by two quadrupoles and ion lenses. The

160   second is the time-of-flight mass analyzer (TOF), where the pressure is approximately 10^{-6}

161   mbar. The sample flow from the chamber was 10 L/min and the core-sampled flow into the

162   APi was 0.8 L/min, with the remaining flow being discarded.

163   There is no direct chemical ionization in front of the instrument. The APi-TOF measures

164   the positive or negative ions and cluster ions as they are present in the ambient atmosphere.

165   As described above, in the CLOUD chamber ions are formed by GCR or deliberately by π+

166   beam, leading to ion concentrations of a few hundred to thousands per cm^3, respectively. In

167   our chamber the dominant ionizing species are NH_4^+ and NO_3^- (see below). These ions

168   mainly form clusters with the organic molecules, which is driven by the cluster energies.

169   Therefore, the signals obtained do not provide a quantitative measure of the concentration of

170   the compounds. The higher the cluster energy with certain compounds the higher the ion

171   cluster concentration will be.

172   We calibrated the APi-TOF using trioctylmethylammonium bis (trifluoromethylsulfonyl)

173   imide (TBMA, $C_{27}H_{54}F_6N_2O_4S_2$) to facilitate the exact ion mass determination in both

174   positive and negative ion modes. We employed two calibration methods, the first one by

175   nebulizing TBMA and separating cluster ions with a high-resolution ultra-fine differential

176   mobility analyzer (UDMA) (see Steiner et al. (2014) for more information); the second one

177   by using electrospray ionization of a TBMA solution. The calibration with the electrospray

178   ionization was performed three times, one for each temperature. These calibrations enabled

179   mass/charge (m/z) measurements with high accuracy up to 1500 Th in the positive ion mode

180   and 900 Th in the negative ion mode.

181   Additionally, two peaks in the positive ion mode were identified as contaminants and also

182   used for calibration purposes at the three different temperatures: $C_{10}H_{14}OH^+$ and $C_{20}H_{28}O_2H^+$.

183   These peaks were present before the addition of ozone in the chamber (therefore being most

184   likely not products of α-pinene ozonolysis) and were also detected by a proton transfer

185   reaction time of flight mass spectrometer (PTR-TOF-MS). Both peaks appeared at the same

186   m/z at all three temperatures. Therefore, based on the calibrations with the UDMA, the

187   electrospray and the two organic calibration peaks, we expect an accurate mass calibration at

188   the three temperatures.

189   2.3. **Experimental conditions**

190   All ambient ion composition data reported here were obtained during nucleation

191 experiments from pure α-pinene ozonolysis. The experiments were conducted under dark

192 conditions, at a relative humidity (RH) of 38% with an O_3 mixing ratio between 33 and 43

193 ppbv (Table 1). The APi-TOF measurements were made under both galactic cosmic ray

194 (GCR) and π^+ beam conditions, with ion-pair concentrations around 700 cm^{-3} and 4000 cm^{-3},

195 respectively.

196

197

198   Table 1. Experiments performed at the CLOUD chamber.

Campaign	Experiment No.	Ionization	α-pinene (pptv)	O_3 (ppbv)	Mass spectrometer polarity	Temperature (˚C)
CLOUD 8	1211.02	GCR	258	33.8	Negative	5
CLOUD 10	1710.04	π^+ beam	618	41.5	Positive	5
CLOUD 10	1712.04	π^+ beam	511	40.3	Negative and positive	25
CLOUD 10	1727.04	π^+ beam	312	43.3	Negative and positive	-25

199

200   2.4. **Quantum chemical calculations**

201   Quantum chemical calculations were performed on the cluster ion formation from the

202 oxidation products of α-pinene. The Gibbs free energies of formation of representative HOM

203 clusters were calculated using the MO62X functional (Zhao and Truhlar, 2008), and the 6-

204 31+G(d) basis set (Ditchfield, 1971) using the Gaussian09 program (Frisch et al., 2009). This

205 method has been previously applied for clusters containing large organic molecules (Kirkby

206 et al., 2016).

207

3. Results and discussion

3.1. Ion composition

Under dry conditions (RH = 0%) and GCR ionization, the main detected positive ions were N_2H^+ and O_2^+. With increasing RH up to ~ 30% we observed the water clusters H_3O^+, $(H_2O)\cdot H_3O^+$ and $(H_2O)_2\cdot H_3O^+$ as well as NH_4^+, $C_5H_5NH^+$ (protonated pyridine), Na^+, and K^+ (Fig. 1A). The concentrations of the precursors of some of the latter ions are expected to be very low: for example, NH_3 mixing ratios were previously found to be in the range of 0.3 pptv (at −25 ˚C), 2 pptv (at 5 ˚C) and 4.3 pptv (at 25 ˚C) (Kürten et al., 2016). However, in a freshly cleaned chamber we expect ammonia levels below 1 pptv also at the higher temperatures. For the negative ions, NO_3^- was the main detected background signal. Before adding any trace gas to the chamber the signal of HSO_4^- was at a level of 1% of the NO_3^- signal (corresponding to $<5\cdot 10^{-4}$ molecules cm^{-3}, Kirkby et al., 2016), excluding any contribution of sulfuric acid to nucleation in our experiments.

After initiating α-pinene ozonolysis, more than 460 different peaks from organic ions were identified in the positive spectrum. The majority of peaks were clustered with NH_4^+, while only 10.2 % of the identified peaks were composed of protonated organic molecules. In both cases the organic core was of the type $C_{7-10}H_{10-16}O_{1-10}$ for the monomer region and $C_{17-20}H_{24-32}O_{5-19}$ for the dimer region.

In the negative spectrum we identified more than 530 HOMs, of which ~62% corresponded to organic clusters with NO_3^- or, to a lesser degree, $HNO_3\cdot NO_3^-$. The rest of the peaks were negatively charged organic molecules. In general, the organic core of the molecules was of the type $C_{7-10}H_{9-16}O_{3-12}$ in the monomer region and $C_{17-20}H_{19-32}O_{10-20}$ in the dimer region. For brevity we refer to the monomer, dimer (and n-mer) as C_{10}, C_{20} and $C_{(10n)}$ respectively. Here, the subscript indicates the maximum number of carbon atoms in these molecules, even though the bands include species with slightly fewer carbon atoms.

3.1.1. Positive spectrum

The positive spectrum is characterized by bands of high intensity at C_{20} intervals, as shown in Fig. 1 B. Although we detected the monomer band (C_{10}), its integrated intensity was

237 much lower than the C_{20} band; furthermore, the trimer and pentamer bands were almost
238 completely absent. Based on chemical ionization mass spectrometry measurements, Kirkby et
239 al. (2016) calculated that the HOM molar yield at 5°C was 3.2% for the ozonolysis of α-
240 pinene, with a fractional yield of 10 to 20% for dimers. A combination reaction of two
241 oxidized peroxy radicals has been previously reported to explain the rapid formation of
242 dimers resulting in covalently bound molecules (see Section 3.3). The pronounced dimer
243 signal with NH_4^+ indicates that (low-volatility) dimers are necessary for positive ion
244 nucleation and initial growth. We observed growth by dimer steps up to C_{80} and possibly
245 even C_{100}. A cluster of two dimers, C_{40}, with a mass/charge in the range of ~ 700 - 1100 Th,
246 has a mobility diameter around 1.5 nm (based on Ehn et al. (2011)).

247   Our observation of HOMs-NH_4^+ clusters implies strong hydrogen bonding between
248 the two species. This is confirmed by quantum chemical calculations which shall be
249 discussed in Section 3.3. Although hydrogen bonding could also be expected between HOMs
250 and H_3O^+, we do not observe such clusters. This probably arises from the higher proton
251 affinity of NH_3, 203.6 kcal/mol, compared with H_2O, 164.8 kcal/mol (Hunter and Lias,
252 1998). Thus, most H_3O^+ ions in CLOUD will transfer their proton to NH_3 to form NH_4^+.

253
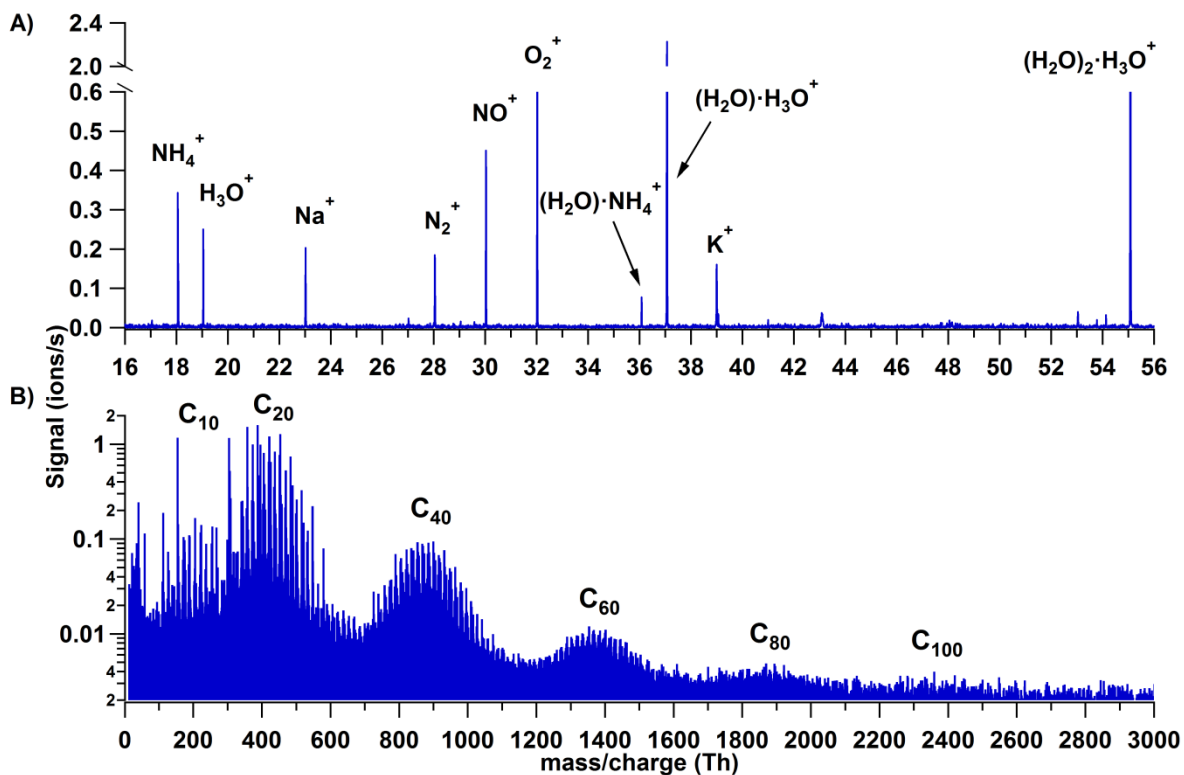
Figure 1. Positive spectra at 5°C. A) Low mass region, where primary ions from galactic cosmic rays are observed, as well as secondary ions such as NH_4^+ which are formed by charge transfer to contaminants. B) Higher mass region during pure biogenic nucleation, which shows broad bands in steps of C_{20}. Most of the peaks represent clusters with NH_4^+.

3.1.2.   Negative spectrum

In the negative spectra, the monomer, dimer and trimer bands are observed during nucleation (Fig. 2). Monomers and dimers have similar signal intensities, whereas the trimer intensity is at least 10 times lower (Fig. 1 A and B). The trimer signal is reduced since it is a cluster of two gas phase species ($C_{10}+C_{20}$). Additionally, a lower transmission in the APi-TOF may also be a reason for the reduced signal.

In Fig. 2, we compare the CLOUD negative-ion spectrum with the one from nocturnal atmospheric measurements from the boreal forest at Hyytiälä as reported by Ehn et al. (2010). Panels 2A and 2B show the negative spectrum of α-pinene ozonolysis in the CLOUD chamber on logarithmic and linear scales, respectively. Panel 2C shows the Hyytiälä

spectrum for comparison. Although the figure shows unit mass resolution, the high resolution analysis confirms the identical composition for the main peaks: $C_8H_{12}O_7 \cdot NO_3^-$, $C_{10}H_{14}O_7 \cdot NO_3^-$, $C_{10}H_{14}O_8 \cdot NO_3^-$, $C_{10}H_{14}O_9 \cdot NO_3^-$, $C_{10}H_{16}O_{10} \cdot NO_3^-$ and $C_{10}H_{14}O_{11} \cdot NO_3^-$ (marked in the monomer region), and $C_{19}H_{28}O_{11} \cdot NO_3$, $C_{19}H_{28}O_{12} \cdot NO_3$, $C_{20}H_{30}O_{12} \cdot NO_3^-$, $C_{19}H_{28}O_{14} \cdot NO_3^-$, $C_{20}H_{30}O_{14} \cdot NO_3$, $C_{20}H_{32}O_{15} \cdot NO_3^-$, $C_{20}H_{30}O_{16} \cdot NO_3^-$, $C_{20}H_{30}O_{17} \cdot NO_3^-$ and $C_{20}H_{30}O_{18} \cdot NO_3^-$ (marked in the dimer region). The close correspondence in terms of composition of the main HOMs from the lab and the field both in the monomer and dimer region indicates a close reproduction of the atmospheric night-time conditions at Hyytiälä by the CLOUD experiment. In both cases the ion composition was dominated by HOMs clustered with NO_3^-. However, Ehn et al. (2010) did not report nocturnal nucleation, possibly because of a higher ambient condensation sink than in the CLOUD chamber.
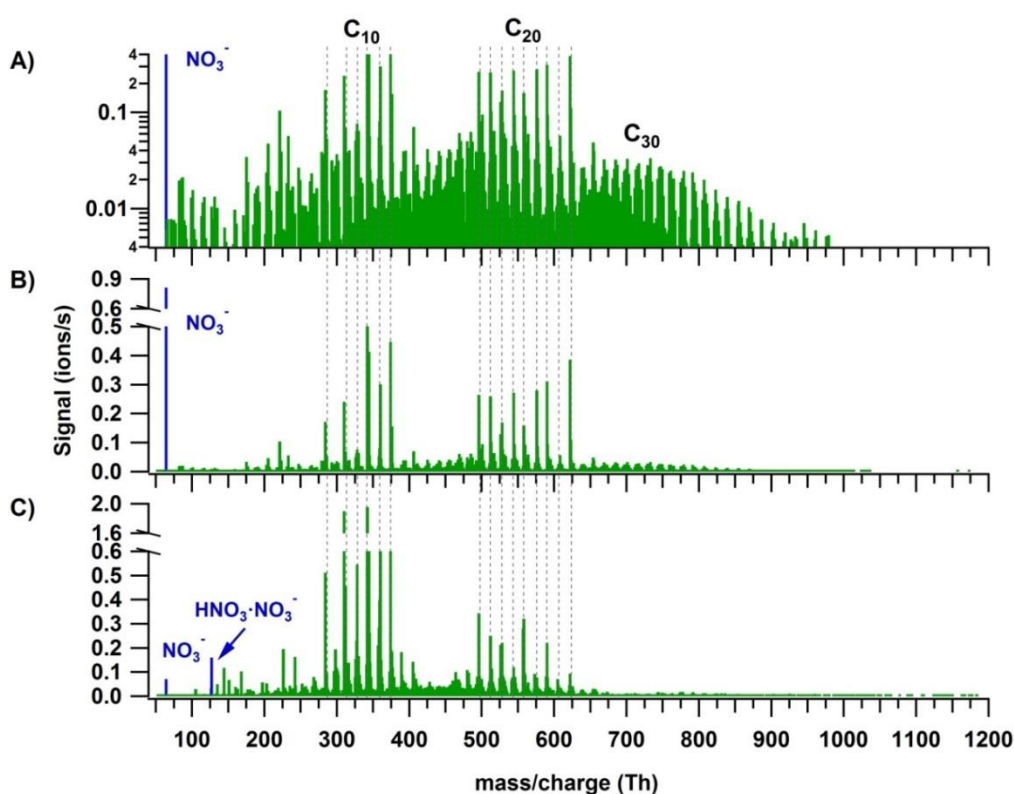
Figure 2. Comparison of the negative ion composition during α-pinene ozonolysis in CLOUD and during night time in the boreal forest at Hyytiälä (Finland). A) CLOUD spectrum on a logarithmic scale. B) CLOUD spectrum on a linear scale. C) Typical night time spectrum from the boreal forest at Hyytiälä (Finland), adapted from Ehn et al. (2010).

287   3.2. **Temperature dependence**

288   Experiments at three different temperatures (25 °C, 5°C and -25 ˚C) were conducted
289   at similar relative humidity and ozone mixing ratios (Table 1 and Fig. 2). Mass defect plots
290   are shown for the same data in Figure 4. The mass defect is the difference between the exact
291   and the integer mass and is shown on the y-axis versus the mass/charge on the x-axis. Each
292   point represents a distinct atomic composition of a molecule or cluster. Although the
293   observations described in the following are valid for both polarities, the trends at the three
294   temperatures are better seen in the positive mass spectra due to a higher sensitivity at high
295   *m/z*.

296   The first point to note is the change in the distribution of the signal intensity seen in
297   Figure 3 (height of the peaks) and in Figure 4 (size of the dots) with temperature. In the
298   positive ion mode, the dimer band has the highest intensity at 25 and 5˚C (see also Fig. 1B),
299   while at -25˚C the intensity of the monomer becomes comparable to that of the dimer. This
300   indicates a reduced rate of dimer formation at -25 ˚C, or that the intensity of the ion signal
301   depends on both the concentration of the neutral compound and on the stability of the ion
302   cluster. Although the monomer concentration is higher than that of the dimers (Tröstl et al.,
303   2016), the C_{20} ions are the more stable ion clusters as they can form more easily two
304   hydrogen bonds with NH_4^+ (see Section 3.3). Thus, positive clusters formed from monomers
305   may not be stable enough at higher temperatures. Moreover, charge transfer to dimers is also
306   favored.
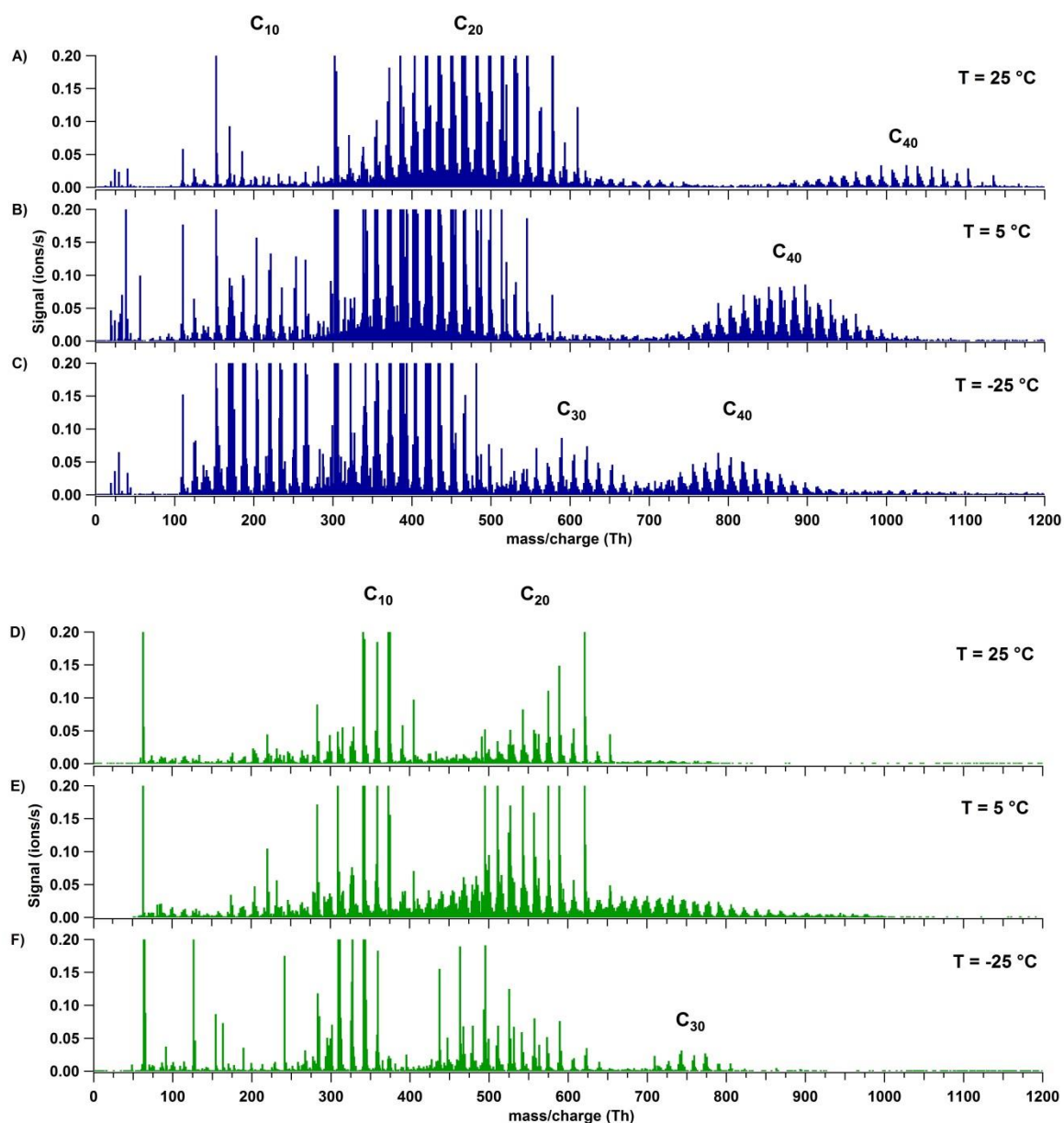
Figure 3. Positive (A-C) and negative (D-F) mass spectra during pure biogenic nucleation induced by ozonolysis of α-pinene) at three temperatures: 25°C (A, D), 5°C (B, E) and -25°C (C, F). A progressive shift towards a lower oxygen content and lower masses is observed in all bands as the temperature decreases. Moreover, the appearance of C_{30} species can be seen in the positive spectrum at the lowest temperature (C).

The data also show a "shift" in all band distributions towards higher masses with increasing temperature, denoting a higher concentration of the more highly oxygenated molecules and the appearance of progressively more oxygenated compounds at higher temperatures. The shift is even more pronounced in the higher mass bands, as clearly seen in

318   the C_{40} band of the positive ion mode in Figure 3 (A-C). In this case the combination of two
319   HOM dimers to a C_{40} cluster essentially doubles the shift of the band towards higher
320   mass/charge at higher temperatures compared to the C_{20} band. Moreover, the width of each
321   band increases with temperature, as clearly seen in the positive ion mode in Figure 4,
322   especially for the C_{40} band. At high temperatures, the production of more highly oxygenated
323   HOMs seems to increase the possible combinations of clusters, resulting in a wider band
324   distribution.

325
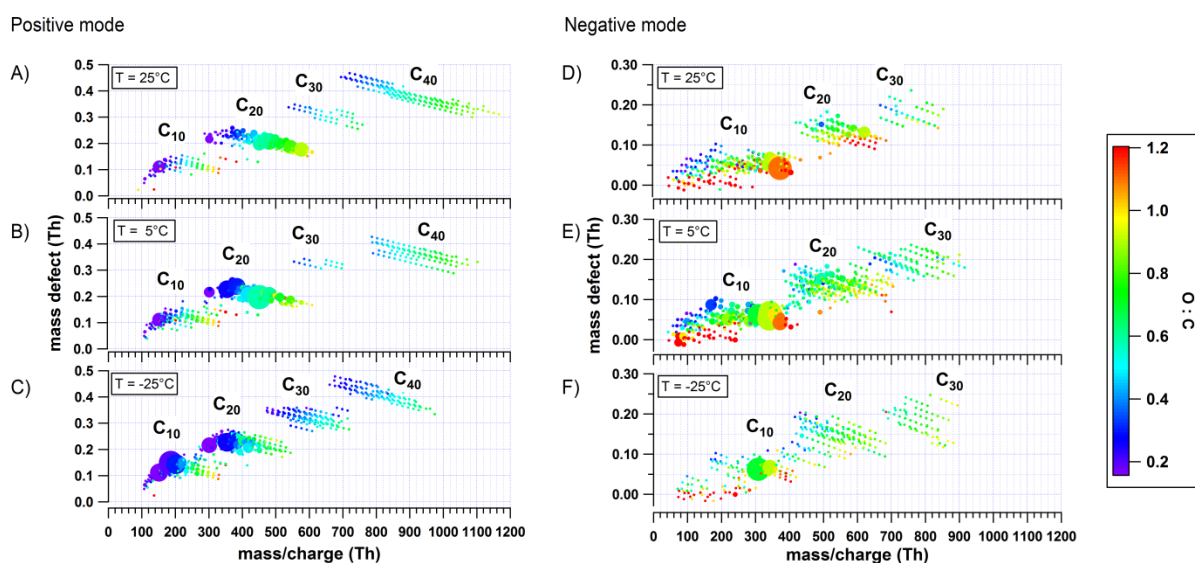
326

327   Figure 4. Mass defect plots with the color code denoting the O:C ratio (of the organic core) at
328   25, 5 and -25°C for positive (A-C) and negative ion mode (D-F). A lower O:C ratio is
329   observed in the positive ion mode than in the negative ion mode. The intensity of the main
330   peaks (linearly proportional to the size of the dots) changes with temperature for both
331   polarities due to a lower degree of oxygenation at lower temperature.

332

333   This trend in the spectra indicates that the unimolecular autoxidation reaction
334   accelerates at higher temperatures in competition to the bimolecular termination reactions
335   with HO_2 and RO_2. This is expected. If unimolecular and bimolecular reactions are
336   competitive, the unimolecular process will have a much higher barrier because the pre-
337   exponential term for a unimolecular process is a vibrational frequency while the pre-

exponential term for the bimolecular process is at most the bimolecular collision frequency, which is four orders of magnitude lower. Quantum chemical calculations determine activation energies between 22.56 and 29.46 kcal/mol for the autoxidation of different $RO_2^.$ radicals from α-pinene (Rissanen et al., 2015). Thus, such a high barrier will strongly reduce the autoxidation rate at the low temperatures.

The change in the rate of autoxidation is also reflected in the O:C ratio, both in the positive ion mode (Figure 4 A-C), and the negative ion mode (D-F), showing a clear increase with increasing temperature. The average O:C ratios (weighted by the peak intensities) are presented in Table 2 for both polarities and the three temperatures, for all the identified peaks (total) and separately for the monomer and dimer bands. For a temperature change from 25 to -25°C the O:C ratio decreases for monomers, dimers and total number of peaks. At high masses (e.g., for the C_{30} and C_{40} bands), the O:C ratio may be slightly biased since accurate identification of the molecules is less straightforward: as an example, $C_{39}H_{56}O_{25} \cdot NH_4^+$ has an exact mass-to-charge ratio of 942.34 Th (O/C = 0.64), which is very similar to $C_{40}H_{60}O_{24} \cdot NH_4^+$ at 942.38 Th (O/C = 0.60). However, such possible misidentification would not influence the calculated total O/C by more than 0.05, and the main conclusions presented here remain robust.

Table 2. Signal weighted average O:C ratios for positive and negative spectra at 25, 5 and -25 °C.

Temperature (°C)	O/C					
	Positive mode			Negative mode		
	Monomer	Dimer	Total	Monomer	Dimer	Total
25	0.37	0.57	0.54	0.94	0.81	0.90
5	0.34	0.51	0.49	0.88	0.66	0.75
-25	0.31	0.38	0.36	0.79	0.65	0.68

The O:C ratios are higher for the negative ions than for the positive ions at any of the three temperatures. Although some of the organic cores are the same in the positive and negative ion mode, the intensity of the peaks of the most oxygenated species is higher in the negative spectra. While the measured O:C ratio ranges between 0.4 and 1.2 in the negative

363   ion mode, it is between 0.1 and 1.2 in the positive ion mode. An O:C ratio of 0.1, which was

364   detected only in the positive ion mode, corresponds to monomers and dimers with two

365   oxygen atoms. The presence of molecules with such low oxygen content was also confirmed

366   with a proton transfer reaction time-of-flight mass spectrometer (PTR-TOF-MS), at least in

367   the monomer region. Ions with O:C ratio less than 0.3 are probably from the main known

368   oxidation products like pinonaldehyde, pinonic acid, etc., but also from minor products like

369   pinene oxide and other not identified compounds yet. It is likely that these molecules, which

370   were detected only in the positive mode, contribute only to the growth of the newly formed

371   particles (if at all) rather than to nucleation, owing to their high volatility (Tröstl et al., 2016).

372   In this sense, the positive spectrum could reveal both the molecules that participate in the new

373   particle formation and those that contribute to growth. The differences in the O:C ratios

374   between the two polarities are a result of the affinities of the organic molecules to form

375   clusters either with NO_3^- or NH_4^+, which, in turn, depends on the molecular structure and the

376   functional groups. Hyttinen et al. (2015) reported the binding energies of selected highly

377   oxygenated products of cyclohexene detected by a nitrate CIMS, finding that the addition of

378   OOH groups to the HOM strengthens the binding of the organic core with NO_3^-. Even when

379   the number of H-bonds between NO_3^- and HOM remains the same, the addition of more

380   oxygen atoms to the organic compound could strengthen the bonding with the NO_3^- ion.

381   Thus, the less oxygenated HOMs were not detected in those experiments, neither in ours, in

382   the negative mode. The binding energies were calculated for the positive mode $HOMs-NH_4^+$

383   and are discussed in Section 3.3.

384   We also tested to which extent the formation of the C_{40} band could be reproduced by

385   permutation of the potential C_{20} clusters weighted by the dimer signal intensity. Figure 5

386   shows the measured spectrum (blue) and two types of modeled tetramers: one combining all

387   peaks from the C_{20} band (light gray) and one combining only those peaks with an organic

388   core with O/C $\geq$ 0.4, i.e. likely non-volatile molecules (dark gray). The better agreement of

389   the latter modeled mass spectrum of the tetramer band with the measured one suggests that

390   only the molecules with O/C $\geq$ 0.4 are able to form the tetramer cluster. This would mean that

391   C_{20} molecules with 2-7 oxygen atoms are likely not to contribute to the nucleation, but only

392   to the growth of the newly formed particles. One has to note that the comparison of modeled

393   and measured spectrum relies on the assumption that the charge distribution of dimers is also

394   reflected in the tetramers.

395
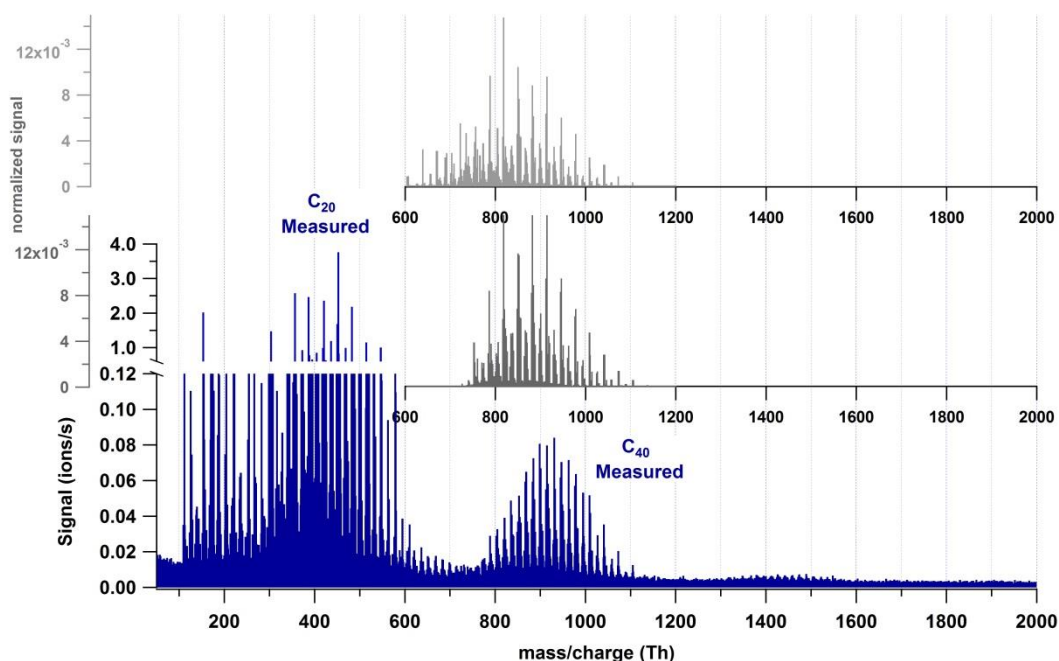
396

397   Figure 5. Comparison of the positive ion mode spectrum measured (blue), the C_{40} band
398   obtained by the combination of all C_{20} molecules (light gray) and the C_{40} band obtained by
399   combination of only the C_{20} molecules with O/C ≥ 0.4 (dark gray). The low or absent signals
400   at the lower masses obtained by permutation suggests that only the highly oxygenated dimers
401   are able to cluster and form C_{40}.

402

403   These two observations (change in signal distribution and band "shift") are not only

404   valid for positive and negative ions, but also for the neutral molecules as observed by two

405   nitrate chemical-ionization atmospheric-pressure-interface time-of-flight mass spectrometers

406   (CI-APi-TOF; Aerodyne Research Inc. and Tofwerk AG). This confirms that there is indeed

407   a change in the HOM composition with different temperature rather than a charge

408   redistribution effect which would only be observed for the ions (APi-TOF). The detailed

409   analysis of the neutral molecules detected by these CI-APi-TOFs will be subject of another

410   paper and is not discussed here.

411   A third distinctive trend in the positive mode spectra at the three temperatures is the

412   increase in signal intensity of the C_{30} band at -25˚C. The increase in the signal of the trimer

413   also seems to occur in the negative ion mode when comparing panels D and F in Figure 3.

414   For this polarity, data from two campaigns were combined (Table **1**). To avoid a bias by

415 possible differences in the APi-TOF settings, we only compare the temperatures from the
416 same campaign, CLOUD 10, therefore experiments at 25 ˚C and -25 ˚C. The increase in the
417 trimer signal may be due to greater stability of the monomer-dimer clusters or even of three
418 C_{10} molecules at low temperatures, as further discussed below.

419

420   3.3. **Quantum chemical calculations**

421   Three points were addressed in the quantum chemical calculations to elucidate the most
422 likely formation pathway for the first clusters, and its temperature dependence. These
423 included (i) the stability of the organic cores with NO_3^- and NH_4^+ depending on the binding
424 functional group, (ii) the difference between charged and neutral clusters in terms of
425 clustering energies, and finally (iii) the possible nature of clusters in the dimer and trimer
426 region.

427   The calculations showed that among the different functional groups the best interacting
428 groups with NO_3^- are in order of importance carboxylic acids (R–C(=O)–OH), hydroxyls (R–
429 OH), peroxy acids (R–C(=O)–O–OH), hydroperoxides (R–O–OH) and carbonyls (R–(R′–)
430 C=O). On the other hand, NH_4^+ preferably forms a hydrogen bond with the carbonyl group
431 independent of which functional group the carbonyl group is linked to: Figure 6 shows
432 examples of NH_4^+ clusters with corresponding free energies of formation for carbonyls (ΔG=
433 -17.98 kcal/mol), carboxylic acid (ΔG= -17.32 kcal/mol), and peroxy acid (ΔG= -17.46
434 kcal/mol). For the three examples shown, the interaction of one hydrogen from NH_4^+ with a
435 C=O group is already very stable with a free energy of cluster ion formation close to -18
436 kcal/mol.

437

438

A

ΔG = -17.98 kcal/mol

B

ΔG = -17,32 kcal/mol

C

ΔG = -17,46 kcal/mol

439
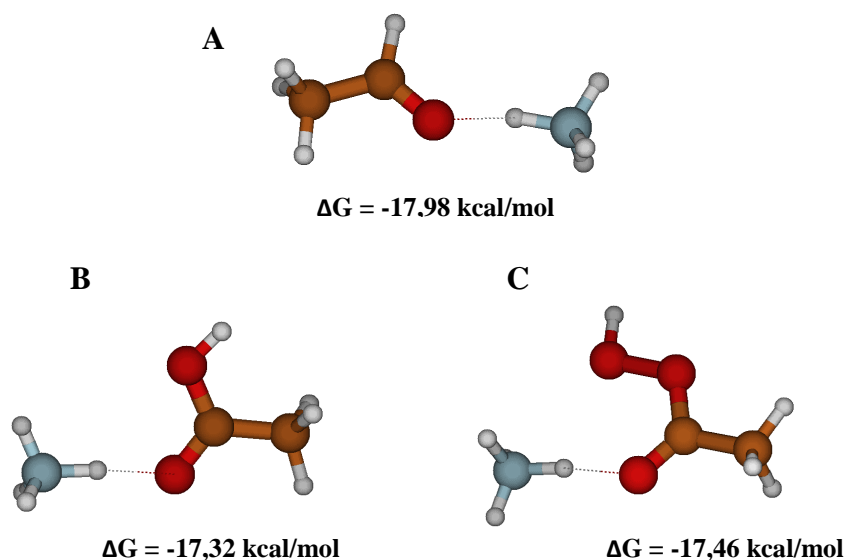
Figure 6. Quantum chemical calculations of the free energy related to the cluster formation between NH_4^+ and three structurally similar molecules with different functional groups: A) acetaldehyde, B) acetic acid and C) peracetic acid.

441

442   To evaluate the effect of the presence of a second C=O to the binding of the organic

443   compound with NH_4^+, we performed a series of calculations with a set of surrogates

444   containing two C=O groups separated by a different number of atoms, as shown in Figure 7.

445   The addition of a second functional group allows the formation of an additional hydrogen-

446   bond, increasing the stability of the cluster considerably (almost two folds) from about -18

447   kcal/mol to -34.07 kcal/mol, whereby the position of the second functional group to form an

448   optimal hydrogen bond (with a 180° angle for N-H-O) strongly influences the stability of the

449   cluster, as can be seen in Figure 7. Thus, optimal separation and conformational flexibility of

450   functional groups is needed to enable an effective formation of two hydrogen bonds with

451   NH_4^+. This could be an explanation for the observation that the signal intensity is higher for

452   dimers than for monomers, as dimers can more easily form two optimal hydrogen bonds with

453   NH_4^+.

454

455

456

457

ΔG = -17,32 kcal/mol

ΔG = -20,81 kcal/mol   **ΔG = -23,43 kcal/mol**

ΔG = -34,07 kcal/mol
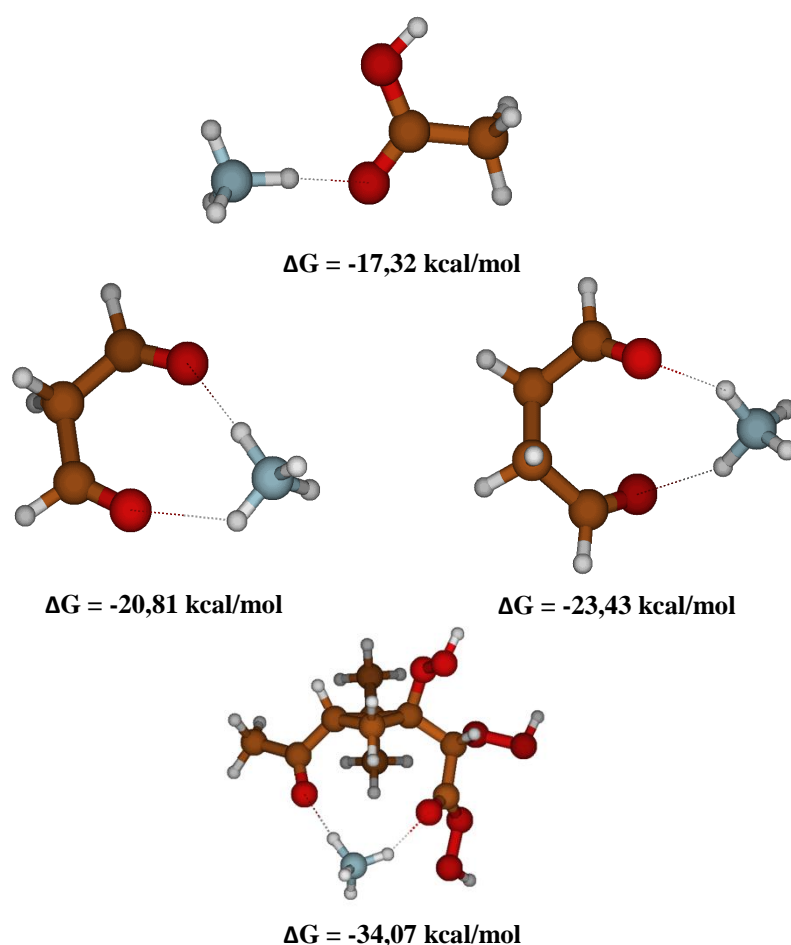
458
459
Figure 7. Quantum chemical calculations for different organic molecules with a carbonyl as the interacting functional group with NH_4^+. Increasing the interacting groups from one to two increases the stability of the cluster. The distance between the interacting groups also influences the cluster stability.

460

461   As shown by Kirkby et al. (2016), ions increase the nucleation rates by one to two
462   orders of magnitudes compared to neutral nucleation. This is expected due to the strong
463   electrostatic interaction between charged clusters. To understand how the stability difference
464   relates to the increase in the nucleation rate, the ΔGs of charged and neutral clusters were
465   compared. For this, $C_{10}H_{14}O_7$ and $C_{20}H_{30}O_{14}$ were selected as representative molecules of the
466   monomer and dimer region, respectively (Kirkby et al., 2016). Table 3 shows the calculated
467   free energies of formation (ΔG) of neutral, positive and negative clusters from these C_{10} and
468   C_{20} molecules at the three temperatures of the experiment. Results show that at 5°C, for

469   example, ΔG of the neutral dimer (C_{10} + C_{10}) is -5.76 kcal/mol while it decreases to -20.95

470   kcal/mol when a neutral and a negative ion form a cluster (C_{10} + C_{10}^-). Similarly, trimers

471   show a substantial increase in stability when they are charged, i.e., from -2.15 kcal/mol to

472   -19.9 kcal/mol, for the neutral and negative cases, respectively. The reduced values of ΔG for

473   the charged clusters (positive and negative) indicate a substantial decrease in the evaporation

474   rate compared to that for neutral clusters, and, therefore, higher stability. Comparing the

475   NH_4^+ and NO_3^- clusters, the energies of formation for the monomer are -22.5 kcal/mol and

476   -25.99 kcal/mol, respectively, showing slightly higher stability for the negative cluster.

477   Inversely, the covalently bound dimer showed greater stability for the positive ion (-30.9

478   kcal/mol) compared to the negative ion (-25.65 kcal/mol).

479

480   Table 3. Gibbs free energies of cluster formation ΔG at three different temperatures. ΔG for
481   the molecules $C_{10}H_{14}O_7$ (C_{10}) and $C_{20}H_{30}O_{14}$ (C_{20}) forming neutral, as well as negative and
482   positive ion clusters.

	Cluster process	*$\Delta G_{-25°C}$ (kcal/mol)*	*$\Delta G_{5°C}$ (kcal/mol)*	*$\Delta G_{25°C}$ (kcal/mol)*
Neutral	C_{10} + C_{10}	-7.3	-5.7	-4.7
	C_{10} + C_{20}	-3.2	-2.1	-1.4
Positive	C_{10} + NH_4^+	-23.4	-22.5	-21.8
	C_{20} + NH_4^+	-31.8	-30.9	-30.2
	C_{10} + C_{10} · NH_4^+	-12.9	-11.7	-10.9
	C_{20} + C_{10} · NH_4^+	-26.0	-24.3	-23.3
	C_{10} + C_{20} · NH_4^+	-17.6	-15.9	-14.8
Negative	C_{10} + C_{10}^-	-22.2	-20.9	-20.1
	C_{20} + C_{10}^-	-21.3	-19.9	-18.9
	C_{10} + NO_3^-	-27.3	-25.9	-25.1
	C_{20} + NO_3^-	-26.9	-25.6	-24.7
	C_{10} + C_{10} · NO_3^-	-11.3	-10.1	-9.2

483

484   The temperature dependence of cluster formation is shown in Figure 8 for the positive ion

485   clusters. The blue and brown solid lines represent the needed ΔG for evaporation-collision

486   equilibrium at 0.3 pptv and 1 pptv HOM mixing ratio, respectively, calculated as described

487   by Ortega et al. (2012). The markers show the calculated formation enthalpies ΔG for each

488   of the possible clusters. For all cases, the trend shows an evident decrease in ΔG with

489   decreasing temperature, with a correspondingly reduced evaporation rate.
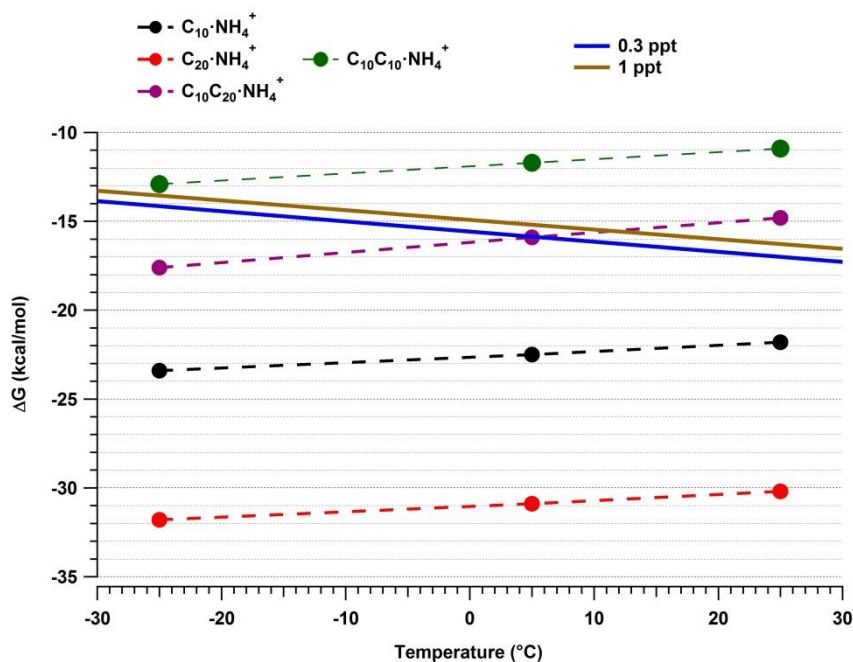
490

491 Figure 8. Quantum chemical calculations of Gibbs free energies for cluster formation at -25,
492 5 and 25°C. Solid lines represent the required ΔG for equilibrium between evaporation and
493 collision rates at 0.3 pptv and 1 pptv of the HOM mixing ratio, respectively. Markers show
494 the ΔG for each cluster (organic core clustered with NH_4^+) at the three temperatures.
495 $C_{10} \cdot NH_4^+$ (black circles) represent the monomer, $C_{20} \cdot NH_4^+$ (red circles) represent the
496 covalently bound dimer, $C_{10}C_{10} \cdot NH_4^+$ (green circles) represent the dimer formed by the
497 clustering of two monomers and $C_{10}C_{20} \cdot NH_4^+$ (purple circles) denote the preferential pathway
498 for the trimer cluster (see Table 3).

499

500 At all three temperatures, the monomer cluster $C_{10} \cdot NH_4^+$ falls well below the equilibrium

501 lines, indicating high stability. Even though the difference between -25°C and 25°C is just

502 -1.6 kcal/mol in free energy, it is enough to produce a substantial difference in the intensity of

503 the band, increasing the signal at least 8-fold at -25°C (as discussed in Section 3.2). In the

504 case of the dimers, we consider the possibility of their formation by collision of a monomer

505 $C_{10} \cdot NH_4^+$ with another C_{10} (resulting in a $C_{10}C_{10} \cdot NH_4^+$ cluster) or the dimer as $C_{20} \cdot NH_4^+$

506 cluster. The calculations show clearly that the cluster $C_{10}C_{10} \cdot NH_4^+$ is not stable at any of the

507 three temperatures (green line). In contrast, the covalently-bound C_{20} forms very stable

508 positive and negative ion clusters (see Table 3). Trimers are mainly observed at lower

509 temperatures. Since the $C_{10}C_{10} \cdot NH_4^+$ cluster is not very stable, we discard the possibility of a

510 trimer formation of the type $C_{10}C_{10}C_{10} \cdot NH_4^+$. Thus, the trimer is likely the combination of a

511 monomer and a covalently-bound dimer ($C_{20}C_{10} \cdot NH_4^+$). According to our calculations (Table

512 3) the preferred evaporation path for this cluster is the loss of C_{10} rather than the evaporation
513 of C_{20}. Therefore, we have chosen to represent only this path in Figure 8. The ΔG of this
514 cluster crosses the evaporation-condensation equilibrium around 5 ˚C and 14 ˚C for a HOM
515 mixing ratio of 0.3 pptv and 1 pptv, respectively, in good agreement with the observed signal
516 increase of the trimer at -25°C (Figure 3 A-C). It is important to note that, due to the
517 uncertainty in the calculations, estimated to be ≤ 2 kcal/mol, we do not consider the crossing
518 as an exact reference.

519 The ΔG of the negative ion clusters, which are also presented in Table 3, decrease
520 similarly to the positive ion clusters by around 2 kcal/mol between 25˚C and -25˚C. The
521 cluster formation energies of the monomer and the dimer with NO_3^- are in agreement with the
522 observed comparable signal intensity in the spectrum (Figure 2) in a similar way as the
523 positive ion clusters. The covalently-bonded dimer ion $C_{20} \cdot NO_3^-$ is also more stable
524 compared to the dimer cluster $C_{10}C_{10} \cdot NO_3^-$, suggesting that the observed composition results
525 from covalently bonded dimers clustering with NO_3^- rather than two individual C_{10} clustering
526 to form a dimer.

527 The formation of a covalently bonded trimer seems unlikely, so the formation of highly
528 oxygenated molecules is restricted to the monomer and dimer region. The trimer could result
529 from the clustering of C_{10} and C_{20} species. Similarly, and based on the C_{20} pattern observed in
530 Figure 1 B, we believe that the formation of the tetramer corresponds to the collision of two
531 dimers. No calculations were done for this case due to the complexity related to the sizes of
532 the molecules, which prevents feasible high level quantum chemical calculations.

533 Finally, a comparison of the ΔG values as presented in Table 3 confirms the expected
534 higher stability of charged clusters compared to neutral clusters, decreasing the evaporation
535 rate of the nucleating clusters and enhancing new particle formation.

536

537 **4. Conclusions**

538 Ions observed during pure biogenic ion-induced nucleation were comprised of mainly
539 organics clustered with NO_3^- and NH_4^+ and to a lesser extent charged organic molecules only
540 or organics clustered with $HNO_3NO_3^-$. We found good correspondence between the negative

541 ions measured in CLOUD with those observed in the boreal forest of Hyytiälä. The observed
542 similarity in the composition of the HOMs in the monomer and dimer region during new-
543 particle formation experiments at CLOUD suggests that pure biogenic nucleation might be
544 possible during night time if the condensation sink is sufficiently low, i.e., comparable to that
545 in the CLOUD chamber, where the wall loss rate for H_2SO_4 is $1.8 \cdot 10^{-3}$ s^{-1} (Kirkby et al.,
546 2016). The positive mass spectrum showed a distinctive pattern corresponding to progressive
547 addition of dimers (C_{20}), up to cluster sizes in the range of stable small particles.

548 Temperature strongly influenced the composition of the detected molecules in several
549 ways. With increasing temperature, a higher oxygen content (O:C ratio) in the molecules was
550 observed in both the positive and the negative mode. This indicates an increase in the
551 autoxidation rate of peroxy radicals which is in competition with their bimolecular
552 termination reactions with HO_2 and RO_2.

553 A broader range of organic molecules was found to form clusters with NH_4^+ than with
554 NO_3^-. Quantum chemical calculations using simplified molecules show that NH_4^+ preferably
555 forms a hydrogen bond with a carbonyl group independently of other functional groups
556 nearby. The addition of a second hydrogen bond was found to increase the cluster stability
557 substantially. Thus, the C_{20}-ions are the more stable ion clusters as they can form more easily
558 two hydrogen bonds with NH_4^+. Although molecules with low oxygen content were
559 measured in the C_{20} band (1 - 4 oxygen atoms), only the molecules with O/C ≥ 0.4 seem to be
560 able to combine to form larger clusters.

561 The quantum chemical calculations showed that the covalently-bonded dimer $C_{20} \cdot$
562 NO_3^- is also more stable than the dimer cluster $C_{10}C_{10} \cdot NO_3^-$, suggesting that the observed
563 composition results from covalently bonded molecules clustering with NO_3^- rather than C_{10}
564 clusters.

565 Temperature affected cluster formation by decreasing evaporation rates at lower
566 temperatures, despite of the lower O:C ratio. In the positive mode a pronounced growth of
567 clusters by addition of C_{20}-HOMs was observed. The formation of a C_{30}-cluster only
568 appeared at the lowest temperature, which was supported by quantum chemical calculations.
569 In the negative mode it appeared as well that the signal of the C_{30}-clusters became stronger
570 with lower temperature. The C_{40}- and higher clusters were probably not seen because of too

571 low sensitivity in this mass range due to the applied instrumental settings. More
572 measurements are needed to determine if the cluster growth of positive and negative ions
573 proceeds in a similar or different way.

574   Nucleation and early growth is driven by the extremely low volatility compounds, i.e.
575 dimers and monomers of high O:C ratios (Tröstl et al., 2016). Here, we observe a reduction
576 of the autoxidation rate leading to oxidation products with lower O:C ratios with decreasing
577 temperature. We expect that this is accompanied by a reduction of nucleation rates. However,
578 a lower temperature reduces evaporation rates of clusters and thereby supports nucleation.
579 The relative magnitude of these compensating effects will be subject of further investigations.

580

581 5. Acknowledgement

582 We would like to thank CERN for supporting CLOUD with important technical and financial
583 resources, and for providing a particle beam from the CERN Proton Synchrotron. We also
584 thank P. Carrie, L.-P. De Menezes, J. Dumollard, K. Ivanova, F. Josa, I. Krasin, R. Kristic, A.
585 Laassiri, O. S. Maksumov, B. Marichy, H. Martinati, S. V. Mizin, R. Sitals, A. Wasem and
586 M. Wilhelmsson for their important contributions to the experiment. This research has
587 received funding from the EC Seventh Framework Programme (Marie Curie Initial Training
588 Network "CLOUD-ITN" no. 215072, MC-ITN "CLOUD-TRAIN" no. 316662, the ERC-
589 Starting grant "MOCAPAF" no. 57360, the ERC-Consolidator grant "NANODYNAMITE"
590 no. 616075 and ERC-Advanced grant "ATMNUCLE" no. 227463), European Union's
591 Horizon 2020 research and innovation programme under the Marie Sklodowska-Curie grant
592 agreement no. 656994, the PEGASOS project funded by the European Commission under the
593 Framework Programme 7 (FP7-ENV-2010-265148), the German Federal Ministry of
594 Education and Research (project nos. 01LK0902A and 01LK1222A), the Swiss National
595 Science Foundation (project nos. 200020_152907, 206021_144947 and 20FI20_159851), the
596 Academy of Finland (Center of Excellence project no. 1118615), the Academy of Finland
597 (135054, 133872, 251427, 139656, 139995, 137749, 141217, 141451, 299574), the Finnish
598 Funding Agency for Technology and Innovation, the Väisälä Foundation, the Nessling
599 Foundation, the University of Innsbruck research grant for young scientists (Cluster
600 Calibration Unit), the Portuguese Foundation for Science and Technology (project no.

CERN/FP/116387/2010), the Swedish Research Council, Vetenskapsrådet (grant 2011-5120), the Presidium of the Russian Academy of Sciences and Russian Foundation for Basic Research (grants 08-02-91006-CERN and 12-02-91522-CERN), the U.S. National Science Foundation (grants AGS1447056, and AGS1439551), and the Davidow Foundation. We thank the *tofTools* team for providing tools for mass spectrometry analysis.

6. References

Almeida, J., Schobesberger, S., Kürten, A., Ortega, I. K., Kupiainen-Määttä, O., Praplan, A. P., Adamov, A., Amorim, A., Bianchi, F., Breitenlechner, M., David, A., Dommen, J., Donahue, N. M., Downard, A., Dunne, E., Duplissy, J., Ehrhart, S., Flagan, R. C., Franchin, A., Guida, R., Hakala, J., Hansel, A., Heinritzi, M., Henschel, H., Jokinen, T., Junninen, H., Kajos, M., Kangasluoma, J., Keskinen, H., Kupc, A., Kurtén, T., Kvashin, A. N., Laaksonen, A., Lehtipalo, K., Leiminger, M., Leppä, J., Loukonen, V., Makhmutov, V., Mathot, S., McGrath, M. J., Nieminen, T., Olenius, T., Onnela, A., Petäjä, T., Riccobono, F., Riipinen, I., Rissanen, M., Rondo, L., Ruuskanen, T., Santos, F. D., Sarnela, N., Schallhart, S., Schnitzhofer, R., Seinfeld, J. H., Simon, M., Sipilä, M., Stozhkov, Y., Stratmann, F., Tomé, A., Tröstl, J., Tsagkogeorgas, G., Vaattovaara, P., Viisanen, Y., Virtanen, A., Vrtala, A., Wagner, P. E., Weingartner, E., Wex, H., Williamson, C., Wimmer, D., Ye, P., Yli-Juuti, T., Carslaw, K. S., Kulmala, M., Curtius, J., Baltensperger, U., Worsnop, D. R., Vehkamäki, H. and Kirkby, J.: Molecular understanding of sulphuric acid-amine particle nucleation in the atmosphere., Nature, 502(7471), 359–63, doi:10.1038/nature12663, 2013.

Andreae, M. O., Afchine, A., Albrecht, R., Amorim Holanda, B., Artaxo, P., Barbosa, H. M. J., Borrmann, S., CecchinI, M. A., Costa, A., Dollner, M., Fütterer, D., Järvinen, E., Jurkat, T., Klimach, T., Konemann, T., Knote, C., Krämer, M., Krisna, T., Machado, L. A. T., Mertes, S., Minikin, A., Pöhlker, C., Pöhlker, M. L., Pöschl, U., Rosenfeld, D., Sauer, D., Schlager, H., Schnaiter, M., Schneider, J., Schulz, C., Spanu, A., Sperling, V. B., Voigt, C., Walser, A., Wang, J., Weinzierl, B., Wendisch, M. and Ziereis, H.: Aerosol characteristics and particle production in the upper troposphere over the Amazon Basin, Atmos. Chem. Phys. Discuss., (August), 2017.

Bianchi, F., Tröstl, J., Junninen, H., Frege, C., Henne, S., Hoyle, C. R., Molteni, U., Herrmann, E., Adamov, A., Bukowiecki, N., Chen, X., Duplissy, J., Gysel, M., Hutterli, M., Kangasluoma, J., Kontkanen, J., Kürten, A., Manninen, H. E., Münch, S., Peräkylä, O., Petäjä, T., Rondo, L., Williamson, C., Weingartner, E., Curtius, J., Worsnop, D. R., Kulmala, M., Dommen, J. and Baltensperger, U.: New particle formation in the free troposphere: A question of chemistry and timing, Science (80-.)., 352(6289), 1109–1112, doi:10.1126/science.aad5456, 2016.

Boucher, O., Randall, D., Artaxo, P., Bretherton, C., Feingold, G., Forster, P., Kerminen, V.-M. V.-M., Kondo, Y., Liao, H., Lohmann, U., Rasch, P., Satheesh, S. K., Sherwood, S., Stevens, B., Zhang, X. Y. and Zhan, X. Y.: Clouds and Aerosols. In: Climate Change 2013: The Physical Science Basis. Contribution of Working Group I to the Fifth Assessment Report

of the Intergovernmental Panel on Climate Change, Clim. Chang. 2013 Phys. Sci. Basis. Contrib. Work. Gr. I to Fifth Assess. Rep. Intergov. Panel Clim. Chang., 571–657, doi:10.1017/CBO9781107415324.016, 2013.

Crounse, J. D., Nielsen, L. B., Jørgensen, S., Kjaergaard, H. G. and Wennberg, P. O.: Autoxidation of organic compounds in the atmosphere, J. Phys. Chem. Lett., 4(20), 3513–3520, doi:10.1021/jz4019207, 2013.

Ditchfield, R.: Self-consistent molecular-orbital methods. IX. An extended gaussian-type basis for molecular-orbital studies of organic molecules, J. Chem. Phys., 54(2), 724, doi:10.1063/1.1674902, 1971.

Dunne, E. M., Gordon, H., Andreas, K., Duplissy, J., Williamson, C., Ortega, I. K., Pringle, K. J., Adamov, A., Baltensperger, U., Barmet, P., Benduhn, F., Bianchi, F., Breitenlechner, M., Clarke, A., Curtius, J., Dommen, J., Donahue, N. M., Ehrhart, S., Flagan, R. C., Franchin, A., Guida, R., Hakala, J., Hansel, A., Heinritzi, M., Jokinen, T., Kangasluoma, J., Kirkby, J., Kulmala, M., Kupc, A., Lawler, M. J., Lehtipalo, K., Makhmutov, V., Mathot, S., Miettinen, P., Nenes, A., Onnela, A., Rap, A., Reddington, C. L. S., Riccobono, F., Richards, N. A. D., Rissanen, M. P., Rondo, L., Sarnela, N., Schobesberger, S., Sengupta, K., Simon, M., Sipil, M., Smith, J. N., Stozkhov, Y. and Tom, A.: Global particle formation from CERN CLOUD measurements, , 2649(October), 1–15, doi:10.1126/science.aaf2649, 2016.

Duplissy, J., Merikanto, J., Franchin, A., Tsagkogeorgas, G., Kangasluoma, J., Wimmer, D., Vuollekoski, H., Schobesberger, S., Lehtipalo, K., Flagan, R. C., Brus, D., Donahue, N. M., Vehkamäki, H., Almeida, J., Amorim, A., Barmet, P., Bianchi, F., Breitenlechner, M., Dunne, E. M., Guida, R., Henschel, H., Junninen, H., Kirkby, J., Kürten, A., Kupc, A., Määttänen, A., Makhmutov, V., Mathot, S., Nieminen, T., Onnela, A., Praplan, A. P., Riccobono, F., Rondo, L., Steiner, G., Tomé, A., Walther, H., Baltensperger, U., Carslaw, K. S., Dommen, J., Hansel, A., Petäjä, T., Sipilä, M., Stratmann, F., Vrtala, A., Wagner, P. E., Worsnop, D. R., Curtius, J. and Kulmala, M.: Effect of ions on sulfuric acid-water binary particle formation: 2. Experimental data and comparison with QC-normalized classical nucleation theory, J. Geophys. Res. Atmos., 121, 1–20, doi:10.1002/2015JD023538, 2016.

Ehn, M., Junninen, H., Petäjä, T., Kurtén, T., Kerminen, V.-M., Schobesberger, S., Manninen, H. E., Ortega, I. K., Vehkamäki, H., Kulmala, M. and Worsnop, D. R.: Composition and temporal behavior of ambient ions in the boreal forest, Atmos. Chem. Phys., 10(17), 8513–8530, doi:10.5194/acp-10-8513-2010, 2010.

Ehn, M., Junninen, H., Schobesberger, S., Manninen, H. E., Franchin, A., Sipilä, M., Petäjä, T., Kerminen, V.-M., Tammet, H., Mirme, A., Mirme, S., Hõrrak, U., Kulmala, M. and Worsnop, D. R.: An instrumental comparison of mobility and mass measurements of atmospheric small ions, Aerosol Sci. Technol., 45(4), 522–532, doi:10.1080/02786826.2010.547890, 2011.

Ehn, M., Kleist, E., Junninen, H., Petäjä, T., Lönn, G., Schobesberger, S., Dal Maso, M., Trimborn, A., Kulmala, M., Worsnop, D. R., Wahner, A., Wildt, J. and Mentel, T. F.: Gas phase formation of extremely oxidized pinene reaction products in chamber and ambient air, Atmos. Chem. Phys., 12(11), 5113–5127, doi:10.5194/acp-12-5113-2012, 2012.

Ehn, M., Thornton, J. a., Kleist, E., Sipilä, M., Junninen, H., Pullinen, I., Springer, M.,

683 Rubach, F., Tillmann, R., Lee, B., Lopez-Hilfiker, F., Andres, S., Acir, I.-H., Rissanen, M.,
684 Jokinen, T., Schobesberger, S., Kangasluoma, J., Kontkanen, J., Nieminen, T., Kurtén, T.,
685 Nielsen, L. B., Jørgensen, S., Kjaergaard, H. G., Canagaratna, M., Maso, M. D., Berndt, T.,
686 Petäjä, T., Wahner, A., Kerminen, V.-M., Kulmala, M., Worsnop, D. R., Wildt, J. and
687 Mentel, T. F.: A large source of low-volatility secondary organic aerosol, Nature, 506(7489),
688 476–479, doi:10.1038/nature13032, 2014.

689 Franchin, A., Ehrhart, S., Leppä, J., Nieminen, T., Gagné, S., Schobesberger, S., Wimmer,
690 D., Duplissy, J., Riccobono, F., Dunne, E. M., Rondo, L., Downard, A., Bianchi, F., Kupc,
691 A., Tsagkogeorgas, G., Lehtipalo, K., Manninen, H. E., Almeida, J., Amorim, A., Wagner, P.
692 E., Hansel, A., Kirkby, J., Kürrten, A., Donahue, N. M., Makhmutov, V., Mathot, S.,
693 Metzger, A., Petäjä, T., Schnitzhofer, R., Sipilä, M., Stozhkov, Y., Tomé, A., Kerminen, V.
694 M., Carslaw, K., Curtius, J., Baltensperger, U. and Kulmala, M.: Experimental investigation
695 of ion-ion recombination under atmospheric conditions, Atmos. Chem. Phys., 15(13), 7203–
696 7216, doi:10.5194/acp-15-7203-2015, 2015.

697 Hirsikko, A., Nieminen, T., Gagné, S., Lehtipalo, K., Manninen, H. E., Ehn, M., Hõrrak, U.,
698 Kerminen, V.-M., Laakso, L., McMurry, P. H., Mirme, A., Mirme, S., Petäjä, T., Tammet,
699 H., Vakkari, V., Vana, M. and Kulmala, M.: Atmospheric ions and nucleation: a review of
700 observations, Atmos. Chem. Phys., 11(2), 767–798, doi:10.5194/acp-11-767-2011, 2011.

701 Hoyle, C. R., Fuchs, C., Jarvinen, E., Saathoff, H., Dias, A., El Haddad, I., Gysel, M.,
702 Coburn, S. C., Trostl, J., Hansel, A., Bianchi, F., Breitenlechner, M., Corbin, J. C., Craven, J.,
703 Donahue, N. M., Duplissy, J., Ehrhart, S., Frege, C., Gordon, H., Hoppel, N., Heinritzi, M.,
704 Kristensen, T. B., Molteni, U., Nichman, L., Pinterich, T., Prevôt, A. S. H., Simon, M.,
705 Slowik, J. G., Steiner, G., Tome, A., Vogel, A. L., Volkamer, R., Wagner, A. C., Wagner, R.,
706 Wexler, A. S., Williamson, C., Winkler, P. M., Yan, C., Amorim, A., Dommen, J., Curtius,
707 J., Gallagher, M. W., Flagan, R. C., Hansel, A., Kirkby, J., Kulmala, M., Mohler, O.,
708 Stratmann, F., Worsnop, D. R. and Baltensperger, U.: Aqueous phase oxidation of sulphur
709 dioxide by ozone in cloud droplets, Atmos. Chem. Phys., 16(3), 1693–1712, doi:10.5194/acp-
710 16-1693-2016, 2016.

711 Hunter, E. P. and Lias, S. G.: Evaluate gas phase basicities and proton affinity of molecules:
712 an update, J. Phys. Chem. Ref. Data, 27(3), 413–656, 1998.

713 Hyttinen, N., Kupiainen-Määttä, O., Rissanen, M. P., Muuronen, M., Ehn, M. and Kurtén, T.:
714 Modeling the charging of highly oxidized cyclohexene ozonolysis products using nitrate-
715 based chemical ionization, J. Phys. Chem. A, 119(24), 6339–6345,
716 doi:10.1021/acs.jpca.5b01818, 2015.

717 Kirkby, J., Curtius, J., Almeida, J., Dunne, E., Duplissy, J., Ehrhart, S., Franchin, A., Gagné,
718 S., Ickes, L., Kürten, A., Kupc, A., Metzger, A., Riccobono, F., Rondo, L., Schobesberger, S.,
719 Tsagkogeorgas, G., Wimmer, D., Amorim, A., Bianchi, F., Breitenlechner, M., David, A.,
720 Dommen, J., Downard, A., Ehn, M., Flagan, R. C., Haider, S., Hansel, A., Hauser, D., Jud,
721 W., Junninen, H., Kreissl, F., Kvashin, A., Laaksonen, A., Lehtipalo, K., Lima, J., Lovejoy,
722 E. R., Makhmutov, V., Mathot, S., Mikkilä, J., Minginette, P., Mogo, S., Nieminen, T.,
723 Onnela, A., Pereira, P., Petäjä, T., Schnitzhofer, R., Seinfeld, J. H., Sipilä, M., Stozhkov, Y.,
724 Stratmann, F., Tomé, A., Vanhanen, J., Viisanen, Y., Vrtala, A., Wagner, P. E., Walther, H.,
725 Weingartner, E., Wex, H., Winkler, P. M., Carslaw, K. S., Worsnop, D. R., Baltensperger, U.
726 and Kulmala, M.: Role of sulphuric acid, ammonia and galactic cosmic rays in atmospheric

727   aerosol nucleation., Nature, 476(7361), 429–33, doi:10.1038/nature10343, 2011.

728   Kirkby, J., Duplissy, J., Sengupta, K., Frege, C., Gordon, H., Williamson, C., Heinritzi, M.,
729   Simon, M., Yan, C., Almeida, J., Tröstl, J., Nieminen, T., Ortega, I. K., Wagner, R., Adamov,
730   A., Amorim, A., Bernhammer, A.-K., Bianchi, F., Breitenlechner, M., Brilke, S., Chen, X.,
731   Craven, J., Dias, A., Ehrhart, S., Flagan, R. C., Franchin, A., Fuchs, C., Guida, R., Hakala, J.,
732   Hoyle, C. R., Jokinen, T., Junninen, H., Kangasluoma, J., Kim, J., Krapf, M., Kürten, A.,
733   Laaksonen, A., Lehtipalo, K., Makhmutov, V., Mathot, S., Molteni, U., Onnela, A., Peräkylä,
734   O., Piel, F., Petäjä, T., Praplan, A. P., Pringle, K., Rap, A., Richards, N. A. D., Riipinen, I.,
735   Rissanen, M. P., Rondo, L., Sarnela, N., Schobesberger, S., Scott, C. E., Seinfeld, J. H.,
736   Sipilä, M., Steiner, G., Stozhkov, Y., Stratmann, F., Tomé, A., Virtanen, A., Vogel, A. L.,
737   Wagner, A. C., Wagner, P. E., Weingartner, E., Wimmer, D., Winkler, P. M., Ye, P., Zhang,
738   X., Hansel, A., Dommen, J., Donahue, N. M., Worsnop, D. R., Baltensperger, U., Kulmala,
739   M., Carslaw, K. S. and Curtius, J.: Ion-induced nucleation of pure biogenic particles, Nature,
740   533(7604), 521–526, doi:10.1038/nature17953, 2016.

741   Kulmala, M., Vehkamäki, H., Petäjä, T., Dal Maso, M., Lauri, A., Kerminen, V. M., Birmili,
742   W. and McMurry, P. H.: Formation and growth rates of ultrafine atmospheric particles: A
743   review of observations, J. Aerosol Sci., 35(2), 143–176, doi:10.1016/j.jaerosci.2003.10.003,
744   2004.

745   Kulmala, M., Kontkanen, J., Junninen, H., Lehtipalo, K., Manninen, H. E., Nieminen, T.,
746   Petäjä, T., Sipilä, M., Schobesberger, S., Rantala, P., Franchin, A., Jokinen, T., Järvinen, E.,
747   Äijälä, M., Kangasluoma, J., Hakala, J., Aalto, P. P., Paasonen, P., Mikkilä, J., Vanhanen, J.,
748   Aalto, J., Hakola, H., Makkonen, U., Ruuskanen, T., Mauldin, R. L., Duplissy, J.,
749   Vehkamäki, H., Bäck, J., Kortelainen, A., Riipinen, I., Kurtén, T., Johnston, M. V, Smith, J.
750   N., Ehn, M., Mentel, T. F., Lehtinen, K. E. J., Laaksonen, A., Kerminen, V.-M. and Worsnop,
751   D. R.: Direct observations of atmospheric aerosol nucleation., Science, 339(6122), 943–6,
752   doi:10.1126/science.1227385, 2013.

753   Kürten, A., Bianchi, F., Almeida, J., Kupiainen-Määttä, O., Dunne, E. M., Duplissy, J.,
754   Williamson, C., Barmet, P., Breitenlechner, M., Dommen, J., Donahue, N. M., Flagan, R. C.,
755   Franchin, A., Gordon, H., Hakala, J., Hansel, A., Heinritzi, M., Ickes, L., Jokinen, T.,
756   Kangasluoma, J., Kim, J., Kirkby, J., Kupc, A., Lehtipalo, K., Leiminger, M., Makhmutov,
757   V., Onnela, A., Ortega, I. K., Petäjä, T., Praplan, A. P., Riccobono, F., Rissanen, M. P.,
758   Rondo, L., Schnitzhofer, R., Schobesberger, S., Smith, J. N., Steiner, G., Stozhkov, Y.,
759   Tomé, A., Tröstl, J., Tsagkogeorgas, G., Wagner, P. E., Wimmer, D., Ye, P., Baltensperger,
760   U., Carslaw, K. S., Kulmala, M. and Curtius, J.: Experimental particle formation rates
761   spanning tropospheric sulfuric acid and ammonia abundances, ion production rates, and
762   temperatures, J. Geophys. Res. Atmos., 121(May), 1–31, doi:10.1002/2015JD023908, 2016.

763   Lehtipalo, K., Rondo, L., Kontkanen, J., Schobesberger, S., Jokinen, T., Sarnela, N., Kürten,
764   A., Ehrhart, S., Franchin, A., Nieminen, T., Riccobono, F., Sipilä, M., Yli-Juuti, T., Duplissy,
765   J., Adamov, A., Ahlm, L., Almeida, J., Amorim, A., Bianchi, F., Breitenlechner, M.,
766   Dommen, J., Downard, A. J., Dunne, E. M., Flagan, R. C., Guida, R., Hakala, J., Hansel, A.,
767   Jud, W., Kangasluoma, J., Kerminen, V.-M., Keskinen, H., Kim, J., Kirkby, J., Kupc, A.,
768   Kupiainen-Määttä, O., Laaksonen, A., Lawler, M. J., Leiminger, M., Mathot, S., Olenius, T.,
769   Ortega, I. K., Onnela, A., Petäjä, T., Praplan, A. P., Rissanen, M. P., Ruuskanen, T. M.,
770   Santos, F. D., Schallhart, S., Schnitzhofer, R., Simon, M., Smith, J. N., Tröstl, J.,
771   Tsagkogeorgas, G., Tomé, A., Vaattovaara, P., Vehkämäki, H., Vrtala, A. E., Wagner, P. E.,

772 Williamson, C., Wimmer, D., Winkler, P. M., Virtanen, A., Donahue, N. M., Carslaw, K. S.,
773 Baltensperger, U., Riipinen, I., Curtius, J., Worsnop, D. R. and Kulmala, M.: The effect of
774 acid-base clustering and ions on the growth of atmospheric nano-particles, Nat. Commun.,
775 (May), 1–9, doi:10.1038/ncomms11594, 2016.

776 Merikanto, J., Spracklen, D. V, Mann, G. W., Pickering, S. J. and Carslaw, K. S.: Impact of
777 nucleation on global CCN, Atmos. Chem. Phys., 8601–8616, 2009.

778 Merikanto, J., Duplissy, J., Määttänen, A., Henschel, H., Donahue, N. M., Brus, D.,
779 Schobesberger, S., Kulmala, M. and Vehkamäki, H.: Effect of ions on sulfuric acid-water
780 binary particle formation I: Theory for kinetic and nucleation-type particle formation and
781 atmospheric implications, J. Geophys. Res. Atmos., 121, 1736–1751,
782 doi:10.1002/2015JD023538, 2016.

783 Metzger, A., Verheggen, B., Dommen, J., Duplissy, J., Prevot, A. S. H., Weingartner, E.,
784 Riipinen, I., Kulmala, M., Spracklen, D. V, Carslaw, K. S. and Baltensperger, U.: Evidence
785 for the role of organics in aerosol particle formation under atmospheric conditions., Proc.
786 Natl. Acad. Sci. U. S. A., 107(15), 6646–51, doi:10.1073/pnas.0911330107, 2010.

787 Nadykto, A. B.: Uptake of neutral polar vapor molecules by charged clusters/particles:
788 Enhancement due to dipole-charge interaction, J. Geophys. Res. Atmos., 108(D23), 4717,
789 doi:10.1029/2003JD003664, 2003.

790 Ortega, I. K., Kupiainen, O., Kurtén, T., Olenius, T., Wilkman, O., McGrath, M. J.,
791 Loukonen, V. and Vehkamäki, H.: From quantum chemical formation free energies to
792 evaporation rates, Atmos. Chem. Phys., 12(1), 225–235, doi:10.5194/acp-12-225-2012, 2012.

793 Praplan, A. P., Schobesberger, S., Bianchi, F., Rissanen, M. P., Ehn, M., Jokinen, T.,
794 Junninen, H., Adamov, A., Amorim, A., Dommen, J., Duplissy, J., Hakala, J., Hansel, A.,
795 Heinritzi, M., Kangasluoma, J., Kirkby, J., Krapf, M., Kürten, A., Lehtipalo, K., Riccobono,
796 F., Rondo, L., Sarnela, N., Simon, M., Tomé, A., Tröstl, J., Winkler, P. M., Williamson, C.,
797 Ye, P., Curtius, J., Baltensperger, U., Donahue, N. M., Kulmala, M. and Worsnop, D. R.:
798 Elemental composition and clustering behaviour of α-pinene oxidation products for different
799 oxidation conditions, Atmos. Chem. Phys., 15(8), 4145–4159, doi:10.5194/acp-15-4145-
800 2015, 2015.

801 Riccobono, F., Schobesberger, S., Scott, C. E., Dommen, J., Ortega, I. K., Rondo, L.,
802 Almeida, J., Amorim, A., Bianchi, F., Breitenlechner, M., David, A., Downard, A., Dunne, E.
803 M., Duplissy, J., Ehrhart, S., Flagan, R. C., Franchin, A., Hansel, A., Junninen, H., Kajos, M.,
804 Keskinen, H., Kupc, A., Kürten, A., Kvashin, A. N., Laaksonen, A., Lehtipalo, K.,
805 Makhmutov, V., Mathot, S., Nieminen, T., Onnela, A., Petäjä, T., Praplan, A. P., Santos, F.
806 D., Schallhart, S., Seinfeld, J. H., Sipilä, M., Spracklen, D. V, Stozhkov, Y., Stratmann, F.,
807 Tomé, A., Tsagkogeorgas, G., Vaattovaara, P., Viisanen, Y., Vrtala, A., Wagner, P. E.,
808 Donahue, N. M., Kirkby, J., Kulmala, M., Worsnop, D. R. and Baltensperger, U.: Oxidation
809 products of biogenic emissions contribute to nucleation of atmospheric particles, Science,
810 344(May), 717–721, 2014.

811 Rissanen, M. P., Kurtén, T., Sipilä, M., Thornton, J. A., Kausiala, O., Garmash, O.,
812 Kjaergaard, H. G., Petäjä, T., Worsnop, D. R., Ehn, M. and Kulmala, M.: Effects of chemical
813 complexity on the autoxidation mechanisms of endocyclic alkene ozonolysis products: From

814 methylcyclohexenes toward understanding α-pinene, J. Phys. Chem. A, 119(19), 4633–4650,
815 doi:10.1021/jp510966g, 2015.

816 Schobesberger, S., Junninen, H., Bianchi, F., Lönn, G., Ehn, M., Lehtipalo, K., Dommen, J.,
817 Ehrhart, S., Ortega, I. K., Franchin, A., Nieminen, T., Riccobono, F., Hutterli, M., Duplissy,
818 J., Almeida, J., Amorim, A., Breitenlechner, M., Downard, A. J., Dunne, E. M., Flagan, R.
819 C., Kajos, M., Keskinen, H., Kirkby, J., Kupc, A., Kürten, A., Kurtén, T., Laaksonen, A.,
820 Mathot, S., Onnela, A., Praplan, A. P., Rondo, L., Santos, F. D., Schallhart, S., Schnitzhofer,
821 R., Sipilä, M., Tomé, A., Tsagkogeorgas, G., Vehkamäki, H., Wimmer, D., Baltensperger, U.,
822 Carslaw, K. S., Curtius, J., Hansel, A., Petäjä, T., Kulmala, M., Donahue, N. M. and
823 Worsnop, D. R.: Molecular understanding of atmospheric particle formation from sulfuric
824 acid and large oxidized organic molecules., Proc. Natl. Acad. Sci. U. S. A., 110(43), 17223–
825 8, doi:10.1073/pnas.1306973110, 2013.

826 Shuman, N. S., Hunton, D. E. and Viggiano, A. A.: Ambient and modified atmospheric ion
827 chemistry: from top to bottom, Chem. Rev., 115(10), 4542–4570, doi:10.1021/cr5003479,
828 2015.

829 Steiner, G., Jokinen, T., Junninen, H., Sipilä, M., Petäjä, T., Worsnop, D., Reischl, G. P. and
830 Kulmala, M.: High-resolution mobility and mass spectrometry of negative ions produced in a
831 241   Am   aerosol   charger,   Aerosol   Sci.   Technol.,   48(3),   261–270,
832 doi:10.1080/02786826.2013.870327, 2014.

833 Suni, T., Kulmala, M., Hirsikko, A., Bergman, T., Laakso, L., Aalto, P. P., Leuning, R.,
834 Cleugh, H. and Zegelin, S.: Formation and characteristics of ions and charged aerosol
835 particles in a native Australian Eucalypt forest, Atmos. Chem. Phys., 8, 129–139, 2008.

836 Tröstl, J., Chuang, W. K., Gordon, H., Heinritzi, M., Yan, C., Molteni, U., Ahlm, L., Frege,
837 C., Bianchi, F., Wagner, R., Simon, M., Lehtipalo, K., Williamson, C., Craven, J. S.,
838 Duplissy, J., Adamov, A., Almeida, J., Bernhammer, A.-K., Breitenlechner, M., Brilke, S.,
839 Dias, A., Ehrhart, S., Flagan, R. C., Franchin, A., Fuchs, C., Guida, R., Gysel, M., Hansel, A.,
840 Hoyle, C. R., Jokinen, T., Junninen, H., Kangasluoma, J., Keskinen, H., Kim, J., Krapf, M.,
841 Kürten, A., Laaksonen, A., Lawler, M. J., Leiminger, M., Mathot, S., Möhler, O., Nieminen,
842 T., Onnela, A., Petäjä, T., Piel, F., Miettinen, P., Rissanen, M. P., Rondo, L., Sarnela, N.,
843 Schobesberger, S., Sengupta, K., Sipilä, M., Smith, J. N., Steiner, G., Tomé, A., Virtanen, A.,
844 Wagner, A. C., Weingartner, E., Wimmer, D., Winkler, P. M., Ye, P., Carslaw, K. S.,
845 Curtius, J., Dommen, J., Kirkby, J., Kulmala, M., Riipinen, I., Worsnop, D. R., Donahue, N.
846 M. and Baltensperger, U.: The role of low-volatility organic compounds for initial particle
847 growth in the atmosphere, Nature, 533, 527–531, doi:doi:10.1038/nature18271, 2016.

848 Zhao, Y. and Truhlar, D. G.: The M06 suite of density functionals for main group
849 thermochemistry, thermochemical kinetics, noncovalent interactions, excited states, and
850 transition elements: Two new functionals and systematic testing of four M06-class
851 functionals and 12 other function, Theor. Chem. Acc., 120(1–3), 215–241,
852 doi:10.1007/s00214-007-0310-x, 2008.

853